

Electronic Structure and Thermoelectric Properties of Half-Heusler Alloys NiTZ

Dhurba R. Jaishi,^{1,2} Nileema Sharma,^{1,2} Bishnu Karki,^{1,2} Bishnu P. Belbase,^{1,2} Rajendra P. Adhikari,³ and Madhav P. Ghimire^{1,2, a)}

¹⁾Central Department of Physics, Tribhuvan University, Kirtipur 44613, Kathmandu, Nepal

²⁾Condensed Matter Physics Research Center (CMPRC), Butwal 32907, Rupandehi, Nepal

³⁾Department of Physics, Kathmandu University, Dhulikhel 45200, Nepal

(Dated: 22 December 2020)

We have investigated the electronic and thermoelectric properties of half-Heusler alloys NiTZ (T = Sc, and Ti; Z = P, As, Sn, and Sb) having 18 valence electron. Calculations are performed by means of density functional theory and Boltzmann transport equation with constant relaxation time approximation, validated by NiTiSn. The chosen half-Heuslers are found to be an indirect band gap semiconductor, and the lattice thermal conductivity is comparable with the state-of-the-art thermoelectric materials. The estimated power factor for NiScP, NiScAs, and NiScSb reveals that their thermoelectric performance can be enhanced by appropriate doping rate. The value of ZT found for NiScP, NiScAs, and NiScSb are 0.46, 0.35, and 0.29, respectively at 1200 K.

I. INTRODUCTION

In the past few decades, researchers have been focused on the investigation of the multi-functional materials, which can be used as various applications such as in spintronics, optoelectronics, thermoelectrics (TE), etc. With the surge in demand for green energy sources, TE materials are extensively taken into considerations for their ability to convert relatively small and waste heat into useful energy at the time of energy consumption. Wide range of materials has been explored for the potential half-metals and TE devices such as organic¹, chalcogenides^{2,3}, skutterudites⁴⁻⁶, oxides⁷⁻¹², hybrid perovskites¹³⁻¹⁵, triple-point metals¹⁶, ternary compounds¹⁷, and half-Heusler (hH) alloys¹⁸⁻²⁹. Among them, Heusler compounds have gained much more attention since their discovery in 1903 due to their simple crystalline structure with fascinating properties that includes magnetism, half metallicity, superconductivity, optoelectronic, piezoelectric semiconductors, thermoelectricity, topological insulators and semimetals³⁰⁻³⁸.

Thermoelectric materials are found applicable in day-to-day lives to fulfill the increasing demand of energy of the globalized society. The highly efficient TE devices (cooler, power generator, temperature sensors, etc) can utilize a large amount of wasted thermal energy to generate electricity and vice-versa^{39,40}. For this, the device needs a larger figure of merit (ZT), which depends on the transport properties^{41,42} defined by

$$ZT = \frac{\alpha^2 \sigma T}{\kappa} \quad (1)$$

where α (V K⁻¹) is the Seebeck coefficient, σ (S m⁻¹) is the electrical conductivity, $\kappa = \kappa_e + \kappa_l$ (W m⁻¹K⁻¹) is thermal conductivity, and T(K) is the absolute temperature. $\alpha^2 \sigma$ is defined as the power factor (PF). The symbol κ_e and κ_l rep-

resents the electronic and lattice thermal conductivity, respectively. The materials having a high value of PF along with the low value of κ are suitable for the efficient TE devices⁴³.

Among others, most of the cubic hH alloys with 18 valence electron count (VEC) exhibits high Seebeck coefficients and are reported as promising materials for TE application due to high electrical conductivity and narrow band gap semiconductors with novel electrical and mechanical properties even at high-temperatures^{19-22,44}. In addition to it, hH alloys contain non-toxic and readily available elements, making them environmentally friendly and more cost effective.

Recent experimental and theoretical investigations on hH alloys are mainly focused on improving their thermoelectric efficiency ZT by tuning the power factor and thermal conductivity. Band gap engineering and fluctuation of carrier concentration around the Fermi level (E_F) in Z position is a widely used method to enhance the power factor, whereas, thermal conductivity can be decreased by alloying or by doping on X or Y site to fluctuate the mass of the carriers introducing impurities and nanostructuring⁴⁵⁻⁴⁸.

From the literatures, we noticed that Ni-based hH alloys with 18-VEC are less investigated. Following the Slater-Pauling's rule, the total magnetic moment for these type of hH alloys should be zero. Thus, the zero moment on Ti or Sc at Y site and P or As or Sb at Z site will give rise to zero moment for the Ni atom at the X site resulting in a non-magnetic system^{49,50}. This motivates us to explore the electronic, TE, and other related properties to confirm if these groups of materials could be suitable for TE devices.

II. COMPUTATIONAL DETAILS

The cubic hH alloys NiTZ (T= Sc, and Ti; Z= P, As, Sn, and Sb) belongs to Cl_b structure with space group $F\bar{4}3m$. It contains three inequivalent atoms forming inter-penetrating fcc sublattices with the Wyckoff positions Ni (1/4, 1/4, 1/4), T (1/2, 1/2, 1/2) and Z (0, 0, 0), respectively as shown in Figure 1. The iso-structural NiTiSn is used here to validate our calculations based on the earlier reported results (both theoretical

^{a)}Electronic mail: madhav.ghimire@cdp.tu.edu.np

and experimental).

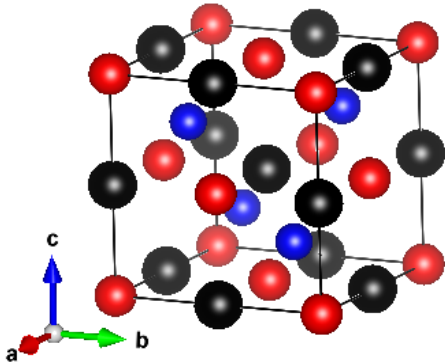


FIG. 1. The crystal structure of cubic hH NiTZ (T= Sc, and Ti; Z= P, As, Sn, and Sb). The balls in blue, black, and red color represents Ni, T, and Z atoms, respectively.

The density functional (DF) calculations has been performed using the full-potential linear augmented plane wave (FP-LAPW) method as implemented in the WIEN2k code⁵¹. We double checked some parts of our calculations using the plane-wave based pseudopotentials Quantum Espresso (QE) package⁵². The standard generalized-gradient approximation (GGA) in the parameterization of Perdew, Burke, and Ernzerhof (PBE)⁵³ was used in scalar-relativistic mode. The modified Becke-Johnson (mBJ) potential⁵⁴ was further included to check the accuracy of the band gaps. The self-consistency convergence criteria for charge was set to $10^{-4}e$, and energy to 10^{-5} Ry.

In the plane-wave pseudopotential approach, we used the norm-conserving pseudopotentials with plane wave cut-off energy for wave function set to 90 Ry. The full Brillouin Zone (BZ) was sampled with an optimized $10 \times 10 \times 10$ mesh of Monkhorst-Pack k -points. To check the dynamical stability, phonon spectrum calculations have been performed with $4 \times 4 \times 4$ q - mesh in phonon BZ, which is based on the DF perturbation theory (DFPT) implemented in the QE package⁵².

The TE properties were calculated using the Boltzmann semi-classical transport equation and constant relaxation time approximation based on a smoothed Fourier interpolation of the bands implemented on BoltzTraP code⁵⁵. The full BZ was sampled with $50 \times 50 \times 50$ k - mesh for the calculation of the transport properties. The electrical conductivity and PF were calculated under constant relaxation time approximation (τ) using the BoltzTraP code based on Boltzmann theory. τ is approximated by fitting the experimental data from Kim *et al.*¹⁸. The lattice thermal conductivity was obtained by solving linearized Boltzmann transport equation (BTE) within the single-mode relaxation time approximation (SMA) using thermal2 code implemented in QE package⁵².

III. RESULTS AND DISCUSSION

A. Structure Optimization and Phonon Stability

We started our calculations by optimizing the cubic hH alloys with $F\bar{4}3m$ symmetry. Our calculated values of lattice parameters and the band gap within GGA and GGA + mBJ are listed in Table I. These values are found to be in fair agreement with the earlier reports of Ma *et al.*⁴⁹ for the GGA case.

TABLE I. The optimized lattice constant a and the band gap E_g within GGA and GGA + mBJ for the cubic hH alloys NiTZ.

System	a (Å)	GGA	GGA+mBJ
		E_g (eV)	E_g (eV)
NiScP	5.69	0.54	0.62
NiScAs	5.84	0.48	0.52
NiScSb	6.12	0.28	0.32
NiTiSn	5.95	0.46	0.45

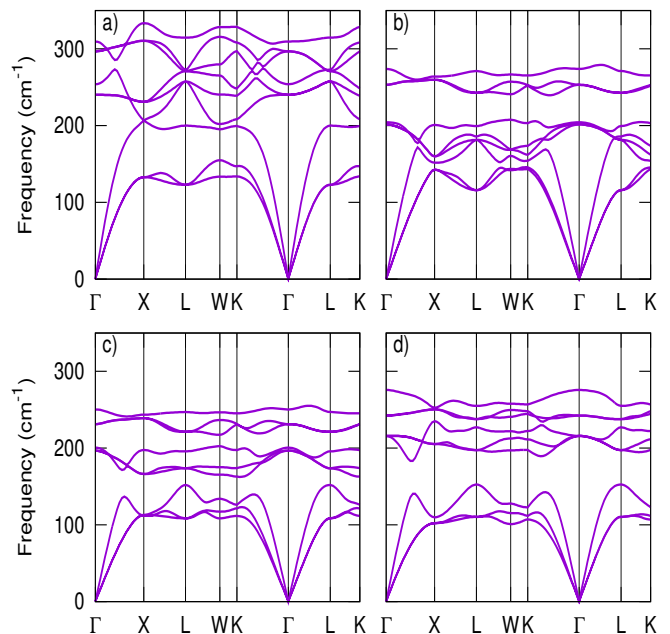


FIG. 2. Phonon band structures for finding the dynamic stability of a) NiScP, b) NiScAs, c) NiScSb, and d) NiTiSn.

The calculated phonon dispersion curves along the high-symmetry points shown in Figure 2 depicts that the proposed hH alloys are thermally stable. This is evidenced by the absence of imaginary phonon frequencies throughout the whole BZ, as expected for dynamic stability⁵⁶. We observed three acoustic (low-frequency region) and six optical phonon (high-frequency region) branches due to three atoms per unit cell.

The majority of the lattice contribution to the thermal conductivity arises from the acoustic part as it has high group velocity compared to the optical part. We found that the acoustical phonon branches of NiScP and NiScAs extends nearly to 200 cm^{-1} while NiScSb and NiTiSn lies within 150 cm^{-1} in frequency. The observation of dynamical stability and preferable energy gap in our proposed hH alloys motivate us to explore the electronic and transport properties for their potential application as TE materials.

B. Electronic Properties

To understand the ground state electronic properties of the material, the total and partial density of states (DOS) are shown in Figure 3. The proposed systems are found to be semiconducting with an energy gap lying within $\sim 0.32 - 0.62 \text{ eV}$, in fair agreement with the earlier report⁴⁹. As seen in the PDOS the main contribution to the total DOS at and around E_F are from the $3d$ -orbitals of Ni and Sc atoms while the contributions from atom on the Z site is negligible (see in Figure 3). This is an indication that doping onto the Z site may improve the carrier concentration. .

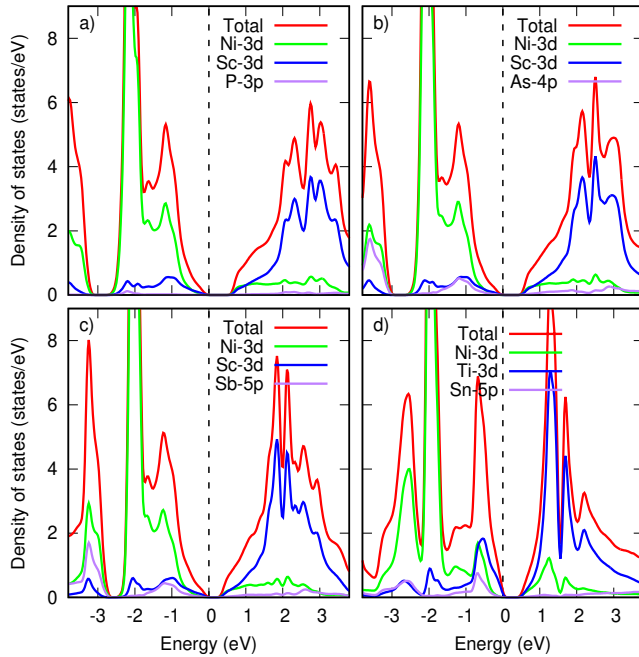


FIG. 3. Total and Partial density of states of a) NiScP, b) NiScAs, c) NiScSb, and d) NiTiSn within GGA + mBJ. Vertical dotted line represent E_F .

It is interesting to note that with increase in the atomic radius of atoms at Z site, say, from P to Sb, the band gap reduces gradually which further leads to the decrease in the hybridization of Ni- $3d$ and Sc- $3d$ states. An indirect band gap is observed in the band structures for hH alloys (see Figure 4) with their valence band maximum (VBM) lying at Γ and conduction band minimum (CBM) at X in the BZ. The VBM

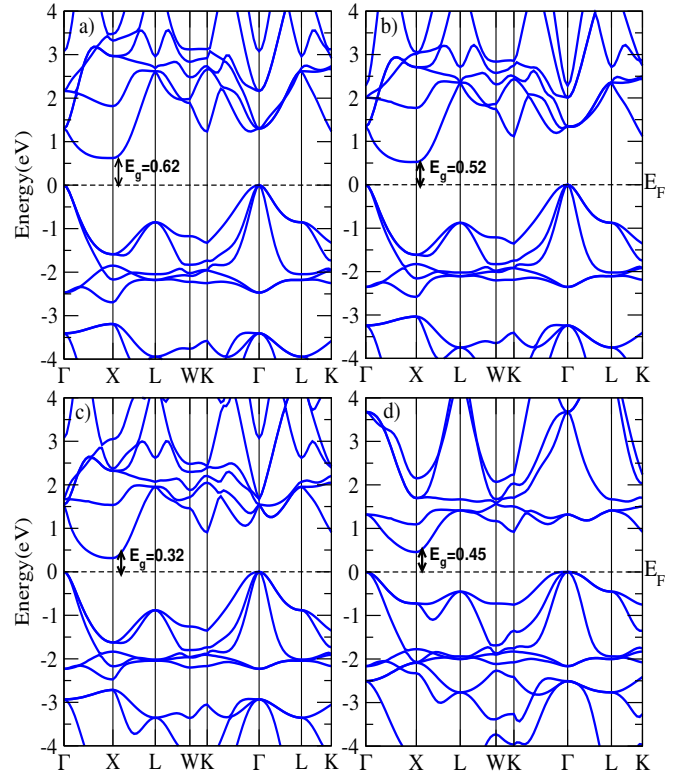


FIG. 4. Electronic band structure of a) NiScP, b) NiScAs, c) NiScSb, and d) NiTiSn within GGA + mBJ.

for the hH alloys are 3-fold degenerate comprising of heavy and light bands. From the observed band structure in Figure 4, the scenario of heavy bands can enhance the Seebeck coefficient, whereas, the light band can facilitate the mobility of charge carriers⁵⁷⁻⁵⁹. Thus, the combination of heavy and light bands are preferable for increasing the TE performance. The band structure shown in Figure 4 (a), (b), and (c) dictates the effective mass to be more at $X - \Gamma$ in CBM than that of VBM at Γ (i.e., the effective mass of electron at CBM is greater than that of the hole at VBM), which play an significant role in TE properties. As seen in NiTiSn (Figure 4 (d)), the VBM (at Γ) is flatter than the CBM (at X) indicating that the effective mass of holes at VBM is more than that of electrons on CBM.

C. Transport Properties

For an efficient TE material, a high value of α and σ with a low κ is expected, as depicted in equation (1). The dimensionless figure of merit ZT can be optimized when these parameters are optimum. But these parameters are inter-related with themselves. Thus, to obtain high value of ZT is insufficient just by tuning one or two parameters. To get insight into the TE properties of hH alloys, we calculate the Seebeck coefficient α , electrical conductivity σ/τ , thermal conductivity ($\kappa = \kappa_e + \kappa_l$), power factor (PF), and the ZT by using constant relaxation time approximation and rigid band approximation.

We first initiate our calculations for NiTiSn by validating

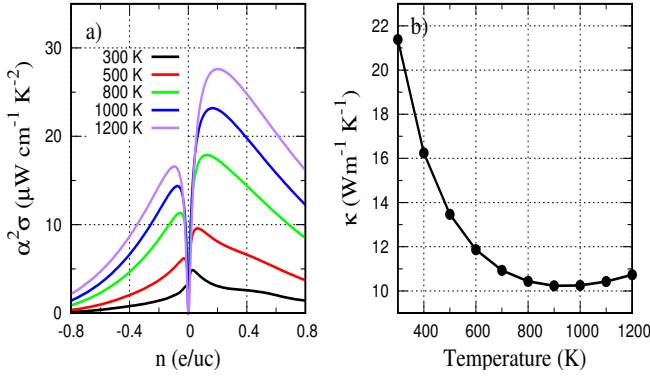


FIG. 5. Power factor as a function of doping level (e/uc) for NiTiSn. The negative (positive) value represents the electron (hole) doping, and b) Total thermal conductivity as a function of temperature.

the theoretical results, such as PF and thermal conductivity with the reported experimental measurements¹⁸. From the comparison of the calculated and experimental electrical conductivity, we approximated the relaxation time $\tau \sim 2 \times 10^{-15}$ s. In the whole process, we use the constant relaxation time, even though it depends on doping level and temperature, obtained for NiTiSn to implement for all the iso-electronic systems.

The PF of NiTiSn was reported to be $\sim 16 \mu\text{Wcm}^{-1}\text{K}^{-2}$ at 700 K, which upon electron doping (by 1% of Sb atom to Sn site), PF rises to $\sim 30 \mu\text{W cm}^{-1}\text{K}^{-2}$. When temperature rises above 700 K, PF is found to decrease in both cases. Comparing these values we estimate that PF may range between $10 - 15 \mu\text{Wcm}^{-1}\text{K}^2$ at 0.04 – 0.06 doping level of electron per unit cell in the same temperature range. In case of hole doping, PF lies within $17 - 23 \mu\text{W cm}^{-1}\text{K}^{-2}$ at the same temperature range when dopants is 0.1 – 0.2 hole per unit cell. This indicates that hole doping is more appropriate than the electrons for PF. The calculated total thermal conductivity $21 - 10 \text{Wm}^{-1}\text{K}^{-1}$ (see Figure 5 (b)) was slightly higher than the earlier report (i.e., $7 - 10 \text{Wm}^{-1}\text{K}^{-1}$), which is mainly due to the electronic contribution found prominent at higher temperature. Our calculated results are comparable with the experimental measurements¹⁸.

The Seebeck coefficient (a, c, e) and the PF (b, d, f) for different level of doping are shown in Figure 6 for NiScP, NiScAs, and NiScSb, respectively. Around E_F (i.e., at $\mu = 0$), the Seebeck coefficient is large ($> \pm 150 \mu\text{V}/\text{K}$), which on doping to either side, falls-off significantly. This is evident from its inverse relation with the carrier concentration.

The optimum values of the doping levels and corresponding TE parameters for 1200 K are listed in Table II.

PF is another parameter to check the reliability of TE materials. As observed in Figure 6, the PF value for p or n -type is significant within the doping range of ± 0.3 . To be specific, at 1000 K the calculated values are approximately 15, 12 and 13 $\mu\text{Wcm}^{-1}\text{K}^{-2}$ for NiScP, NiScAs, and NiScSb within 0.02 – 0.04 hole per unit cell reaching its maximum value at 1200 K. Similarly, for doping range 0.06 – 0.07 electron per unit cell, PF rises to $\sim 27, 25,$ and $20 \mu\text{Wcm}^{-1}\text{K}^{-2}$

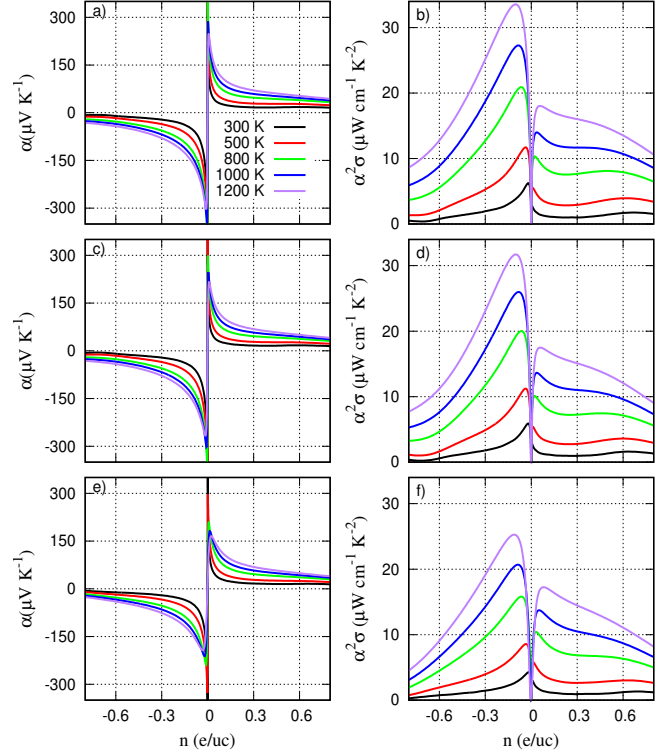


FIG. 6. The Seebeck coefficient (a, c, e) and the Power factor (b, d, f) vs the doping level (in e/uc) at various temperature for NiScP, NiScAs, and NiScSb, respectively. The values in negative (positive) values on the horizontal axes represents the electron (hole) doping, respectively.

at 1000 K, respectively. The sizable value of PF within the doping range 0.07 – 0.08 electron per unit cell suggests that these material could be a good TE materials.

We further show the variation of PF with the chemical potential, μ , in Figure 7. The peak values of PF noted in the chemical potential ranges between 0.4 – 0.7 eV for NiScP, NiScAs and NiScSb. In contrast, the peak value of PF are around -0.2 eV for NiTiSn. From the above scenario, electron doping is found to be more suitable for NiScP, NiScAs, and NiScSb due to larger effective mass of electrons to get better TE performance. This indicates the presence of larger electron pockets resulting in the dense carriers which are confined on the CBM along $\Gamma - X$ (Fig. 4a-c). On the otherhand, in NiTiSn, hole doping is much more favorable due to the higher effective mass of holes resulting from the nearly flatter band in the VBM and CBM along $\Gamma - X$ (see band structure in Fig. 4d).

Figure 8 shows the calculated thermal conductivity as a function of temperature for NiScP, NiScAs, NiScSb, and NiTiSn, respectively. The total thermal conductivity consists of two components *viz.* electronic (κ_e) and lattice (κ_l) parts. At low temperature (say 300 K), the lattice part was found dominant over the electronic part, and with rise in temperature (say upto ~ 900 K, except NiScP), the lattice thermal conductivity and the overall conductivity decreases uniformly.

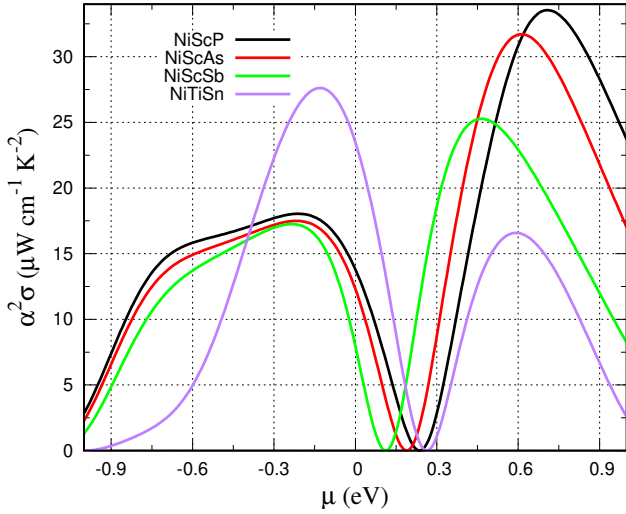


FIG. 7. The power factor vs chemical potential (μ) at 1200 K temperature. The values of chemical potential in negative (positive) represents the hole (electron) doping.

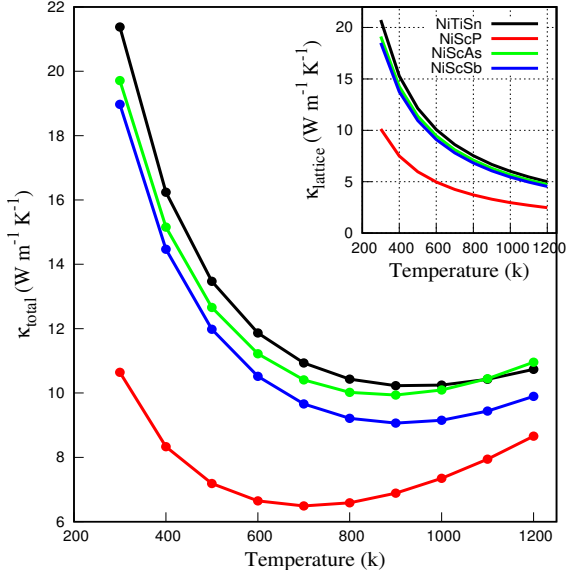


FIG. 8. Total thermal conductivity (κ) as a function of temperature, inset dictates lattice contribution to thermal conductivity (κ_l) of NiScP, NiScAs, NiScSb, and NiTiSn.

To note is, with an increase in temperature starting from 300 K, the carrier concentration increases resulting in higher electrical conductivity, and hence the overall thermal conductivity. Similar features was observed in the recent report of CoMnSb⁶⁰. The calculated lattice conductivity are 10.6, 19, and 18.5 $\text{W m}^{-1}\text{K}^{-1}$ at 300 K which reduces abruptly to 2.5, 4.7, and 4.5 $\text{W m}^{-1}\text{K}^{-1}$ at 1200 K for NiScP, NiScAs, and NiScSb, respectively.

The figure of merit ZT for hH alloys is as shown in Figure 9. With low value (say, 0.05) of ZT at 300 K, it is found to rise linearly with the increase in temperature. At 1200 K,

TABLE II. Calculated optimal doping levels and the corresponding Seebeck coefficient, electrical conductivity, power factor, and ZT of NiTZ ($T = \text{Sc, and Ti; } Z = \text{P, As, Sn, and Sb}$) in cubic symmetry $F\bar{4}3m$ at 1200 K. Negative (-) sign indicates the n -type characteristics.

System	n	α	σ	$\alpha^2\sigma$	ZT
	e/uc	μVK^{-1}	$(\times 10^3 \text{ S cm}^{-1})$	$\mu\text{Wcm}^{-1}\text{K}^{-2}$	
NiTiSn	0.20	154	1.15	27.61	0.30
NiScP	-0.08	-177	1.05	33.16	0.46
NiScAs	-0.08	-168	1.12	31.50	0.35
NiScSb	-0.07	-163	0.90	24.20	0.29

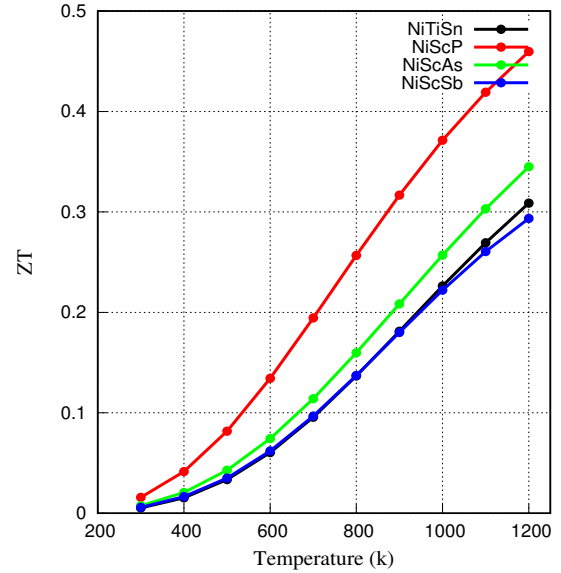


FIG. 9. The ZT as a function of temperature.

the calculated values are 0.30, 0.45, 0.35 and 0.29, respectively for NiTiSn, NiScP, NiScAs, and NiScSb alloys. On the otherhand, the values of total thermal conductivity is found minimum at ~ 700 K for NiScP and ~ 900 K for the remaining systems which starts increases afterwards due to the dominance of electronic part. The variation of ZT with temperature shows linear nature. PF is dominant at higher temperature range due to the increase in carrier concentration along with the electrical conductivity. The observed ZT is low mainly due to a higher value of κ . Even if our ZT values are lower than the commercialized TE materials such as Bi_2Te_3 and PbTe but can be enhanced by means of doping to any of the three atomic sites. Though the ZT value is low (~ 0.05) for the pristine systems compared to the widely used doped Bi-based alloys, say, Bi_2Se_3 ($\sim 0.01 - 0.05$)⁶¹, Bi_2Se_3 at Bi_2Te_3 (~ 0.7)⁶², and Bi-Sb alloys (~ 0.4)⁶³, it can be enhanced by electron doping⁶⁴.

As observed from the calculations above, ZT value can increase when PF is enhanced while minimizing the thermal conductivity. The possible route to tune this from DF is by

proper tuning of the band gap with appropriate electron/hole doping as discussed.

IV. CONCLUSIONS

On the basis on density functional calculations, we investigate the half-Heuslers NiTiSn, NiScP, NiScAs, and NiScSb, respectively. Electronic properties reveal that these materials are semiconductor with an indirect band gap. The narrow-band gap marks them as suitable candidate for TE performance. The calculated power factor shows large value in both the electron and hole doping case. Electron doping is found more preferable than hole for NiScP, NiScAs, and NiScSb, while hole doping is preferable for NiTiSn. Based on the constant relaxation time approximation and rigid band approximation with sizable ZT , these compounds are predicted as a possible TE materials.

ACKNOWLEDGMENTS

MPG acknowledges the Department of Science and Technology, India for awarding the India Science and Research Fellowship (ISRF-2019) with grant number DO/CCSTDS/201/2019, and Alexander von Humboldt Foundation, Germany for the equipment subsidy grants. Part of this work was performed at IIT-Roorkee, India during the ISRF-2019 program, and part of it with the computational resources provided by the Kathmandu University Super-computer Center established with the equipment donated by CERN. MPG thanks H. C. Kandpal for fruitful discussions suggesting half-Heusler group to explore and also for all the logistic and technical supports at IIT-Roorkee.

DATA AVAILABILITY

The data that support the findings of this study are available with the corresponding author and can be obtained upon reasonable request.

DECLARATION OF COMPETING INTEREST

There is no conflict of interest.

- ¹B. Russ, A. Glauddell, J. J. Urban, M. L. Chabiny, and R. A. Segalman, "Organic thermoelectric materials for energy harvesting and temperature control," *Nature Reviews Materials* **1**, 1–14 (2016).
- ²M. G. Kanatzidis, "Nanostructured thermoelectrics: the new paradigm?" *Chemistry of materials* **22**, 648–659 (2010).
- ³G. J. Snyder and E. S. Toberer, "Complex thermoelectric materials," in *materials for sustainable energy: a collection of peer-reviewed research and review articles from Nature Publishing Group* (World Scientific, 2011) pp. 101–110.
- ⁴Y. Lan, A. J. Minnich, G. Chen, and Z. Ren, "Enhancement of thermoelectric figure-of-merit by a bulk nanostructuring approach," *Advanced Functional Materials* **20**, 357–376 (2010).

- ⁵J. R. Szczech, J. M. Higgins, and S. Jin, "Enhancement of the thermoelectric properties in nanoscale and nanostructured materials," *Journal of Materials Chemistry* **21**, 4037–4055 (2011).
- ⁶A. Shankar, D. Rai, M. Ghimire, R. Thapa, *et al.*, "Electronic structure and thermoelectricity of filled skutterudite eu₄ as 12: a dft calculation," *Indian Journal of Physics* **91**, 17–23 (2017).
- ⁷M. Ghimire, Sandeep, and R. Thapa, "Study of the electronic properties of cro₂ using density functional theory," *Modern Physics Letters B* **24**, 2187–2193 (2010).
- ⁸M. P. Ghimire, R. Thapa, D. Rai, Sandeep, T. Sinha, and X. Hu, "Half metallic ferromagnetism in tri-layered perovskites sr₄t₃o₁₀ (t = co, rh)," *Journal of Applied Physics* **117**, 063903 (2015).
- ⁹M. P. Ghimire and X. Hu, "Compensated half metallicity in osmium double perovskite driven by doping effects," *Materials Research Express* **3**, 106107 (2016).
- ¹⁰P. Roy, V. Waghmare, and T. Maiti, "Environmentally friendly ba_xsr_{2-x}tifeo₆ double perovskite with enhanced thermopower for high temperature thermoelectric power generation," *RSC Advances* **6**, 54636–54643 (2016).
- ¹¹W. S. Choi, H. K. Yoo, and H. Ohta, "Polaron transport and thermoelectric behavior in la-doped str_{1-x}o₃ thin films with elemental vacancies," *Advanced Functional Materials* **25**, 799–804 (2015).
- ¹²S. R. Bhandari, D. Yadav, B. Belbase, M. Zeeshan, B. Sadhukhan, D. Rai, R. Thapa, G. Kaphle, and M. P. Ghimire, "Electronic, magnetic, optical and thermoelectric properties of ca₂cr_{1-x}ni_xoso₆ double perovskites," *RSC Advances* **10**, 16179–16186 (2020).
- ¹³A. Filippetti, C. Caddeo, P. Delugas, and A. Mattoni, "Appealing perspectives of hybrid lead-iodide perovskites as thermoelectric materials," *The Journal of Physical Chemistry C* **120**, 28472–28479 (2016).
- ¹⁴C. Lee, J. Hong, A. Stroppa, M.-H. Whangbo, and J. H. Shim, "Organic-inorganic hybrid perovskites abi₃ (a = ch₃ nh₃, nh₂ chnh₂; b = sn, pb) as potential thermoelectric materials: a density functional evaluation," *RSC Advances* **5**, 78701–78707 (2015).
- ¹⁵Y. Liu, X. Li, J. Wang, L. Xu, and B. Hu, "An extremely high power factor in seebeck effects based on a new n-type copper-based organic/inorganic hybrid c₆h₄nh₂cubr₂ film with metal-like conductivity," *Journal of Materials Chemistry A* **5**, 13834–13841 (2017).
- ¹⁶S. Singh, Q. Wu, C. Yue, A. H. Romero, and A. A. Soluyanov, "Topological phonons and thermoelectricity in triple-point metals," *Phys. Rev. Materials* **2**, 114204 (2018).
- ¹⁷D. Rai, A. Shankar, A. P. Sakhya, T. Sinha, P. Grima-Gallardo, H. Cabrera, R. Khenata, M. P. Ghimire, R. Thapa, *et al.*, "Electronic, optical and thermoelectric properties of bulk and surface (001) cunte₂: A first principles study," *Journal of Alloys and Compounds* **699**, 1003–1011 (2017).
- ¹⁸S.-W. Kim, Y. Kimura, and Y. Mishima, "High temperature thermoelectric properties of tin-based half-Heusler compounds," *Intermetallics* **15**, 349–356 (2007).
- ¹⁹C. Fu, S. Bai, Y. Liu, Y. Tang, L. Chen, X. Zhao, and T. Zhu, "Realizing high figure of merit in heavy-band p-type half-Heusler thermoelectric materials," *Nature communications* **6**, 1–7 (2015).
- ²⁰H. Zhu, R. He, J. Mao, Q. Zhu, C. Li, J. Sun, W. Ren, Y. Wang, Z. Liu, Z. Tang, *et al.*, "Discovery of zrcob₂ based half Heuslers with high thermoelectric conversion efficiency," *Nature communications* **9**, 1–9 (2018).
- ²¹H. Zhu, J. Mao, Y. Li, J. Sun, Y. Wang, Q. Zhu, G. Li, Q. Song, J. Zhou, Y. Fu, *et al.*, "Discovery of tafesb-based half-Heuslers with high thermoelectric performance," *Nature communications* **10**, 1–8 (2019).
- ²²T. Graf, P. Klaer, J. Barth, B. Balke, H.-J. Elmers, and C. Felser, "Phase separation in the quaternary Heusler compound coti_{1-x}mn_xsb a reduction in the thermal conductivity for thermoelectric applications," *Scripta Materialia* **63**, 1216–1219 (2010).
- ²³M.-S. Lee, F. P. Poudeu, and S. D. Mahanti, "Electronic structure and thermoelectric properties of sb-based semiconducting half-Heusler compounds," *Phys. Rev. B* **83**, 085204 (2011).
- ²⁴M. Zeeshan, T. Nautiyal, J. van den Brink, and H. C. Kandpal, "Fetasb and femtisb as promising thermoelectric materials: An ab initio approach," *Physical Review Materials* **2**, 065407 (2018).
- ²⁵S. Singh, M. Zeeshan, U. Singh, J. van den Brink, and H. C. Kandpal, "First-principles investigations of orthorhombic-cubic phase transition and its effect on thermoelectric properties in cobalt-based ternary alloys," *Journal of Physics: Condensed Matter* **32**, 055505 (2019).

- ²⁶M. Zeeshan, H. K. Singh, J. van den Brink, and H. C. Kandpal, "Ab initio design of new cobalt-based half-Heusler materials for thermoelectric applications," *Phys. Rev. Materials* **1**, 075407 (2017).
- ²⁷M. Zeeshan, J. van den Brink, and H. C. Kandpal, "Hole-doped cobalt-based Heusler phases as prospective high-performance high-temperature thermoelectrics," *Phys. Rev. Materials* **1**, 074401 (2017).
- ²⁸S. Singh, M. Zeeshan, J. v. d. Brink, and H. C. Kandpal, "Ab initio study of bi-based half Heusler alloys as potential thermoelectric prospects," arXiv:1904.02488 (2019).
- ²⁹D. Rai, A. Shankar, M. Ghimire, R. Khenata, R. Thapa, *et al.*, "Study of the enhanced electronic and thermoelectric (te) properties of $\text{ZrHf}_{1-x}\text{Yt}_{x}$ system: a first principles study," *RSC Advances* **5**, 95353–95359 (2015).
- ³⁰S. Sakurada and N. Shutoh, "Effect of Ti substitution on the thermoelectric properties of (Zr, Hf) NiSn half-Heusler compounds," *Applied Physics Letters* **86**, 082105 (2005).
- ³¹A. Roy, J. W. Bennett, K. M. Rabe, and D. Vanderbilt, "Half-Heusler semiconductors as piezoelectrics," *Phys. Rev. Lett.* **109**, 037602 (2012).
- ³²Z. H. Liu, H. N. Hu, G. D. Liu, Y. T. Cui, M. Zhang, J. L. Chen, G. H. Wu, and G. Xiao, "Electronic structure and ferromagnetism in the martensitic transformation material Ni_2FeGa ," *Phys. Rev. B* **69**, 134415 (2004).
- ³³W. Feng, D. Xiao, Y. Zhang, and Y. Yao, "Half-Heusler topological insulators: A first-principles study with the Tran-Blaha modified Becke-Johnson density functional," *Phys. Rev. B* **82**, 235121 (2010).
- ³⁴R. A. de Groot, F. M. Mueller, P. G. v. Engen, and K. H. J. Buschow, "New class of materials: Half-metallic ferromagnets," *Phys. Rev. Lett.* **50**, 2024–2027 (1983).
- ³⁵M. Ghimire, Sandeep, T. Sinha, and R. Thapa, "First principles study of the electronic and magnetic properties of semi-Heusler alloys Ni_2Sb ($x = \text{Ti, V, Cr}$ and Mn)," *Journal of alloys and compounds* **509**, 9742–9752 (2011).
- ³⁶Sandeep, M. Ghimire, D. Deka, D. Rai, A. Shankar, and R. Thapa, "Magnetic and electronic properties of half-metallic Ni_2Sb : a first principles study," *Indian Journal of Physics* **86**, 301–305 (2012).
- ³⁷Y. Nakajima, R. Hu, K. Kirshenbaum, A. Hughes, P. Syers, X. Wang, K. Wang, R. Wang, S. R. Saha, D. Pratt, *et al.*, "Topological PdBi half-Heusler semimetals: A new family of noncentrosymmetric magnetic superconductors," *Science advances* **1**, e1500242 (2015).
- ³⁸J. Zhang, J. Chen, P. Li, C. Zhang, Z. Hou, Y. Wen, Q. Zhang, W. Wang, and X. Zhang, "Topological electronic state and anisotropic Fermi surface in half-Heusler GdPtBi ," *Journal of Physics: Condensed Matter* **32**, 355707 (2020).
- ³⁹V. Zaitsev, M. Fedorov, I. Eremin, E. Gurieva, and D. Rowe, "Thermoelectrics handbook: macro to nano," CRC Press, Taylor & Francis, Boca Raton (2006).
- ⁴⁰S. B. Riffat and X. Ma, "Thermoelectrics: a review of present and potential applications," *Applied thermal engineering* **23**, 913–935 (2003).
- ⁴¹Y. Pei, X. Shi, A. LaLonde, H. Wang, L. Chen, and G. J. Snyder, "Convergence of electronic bands for high performance bulk thermoelectrics," *Nature* **473**, 66–69 (2011).
- ⁴²A. D. LaLonde, Y. Pei, H. Wang, and G. J. Snyder, "Lead telluride alloy thermoelectrics," *Materials today* **14**, 526–532 (2011).
- ⁴³J. R. Sootsman, D. Y. Chung, and M. G. Kanatzidis, "New and old concepts in thermoelectric materials," *Angewandte Chemie International Edition* **48**, 8616–8639 (2009).
- ⁴⁴C. Felser, G. H. Fecher, and B. Balke, "Spintronics: a challenge for materials science and solid-state chemistry," *Angewandte Chemie International Edition* **46**, 668–699 (2007).
- ⁴⁵J. P. Heremans, V. Jovovic, E. S. Toberer, A. Saramat, K. Kurosaki, A. Charoenphakdee, S. Yamanaka, and G. J. Snyder, "Enhancement of thermoelectric efficiency in PbTe by distortion of the electronic density of states," *Science* **321**, 554–557 (2008).
- ⁴⁶L.-D. Zhao, S.-H. Lo, Y. Zhang, H. Sun, G. Tan, C. Uher, C. Wolverton, V. P. Dravid, and M. G. Kanatzidis, "Ultralow thermal conductivity and high thermoelectric figure of merit in SnSe crystals," *Nature* **508**, 373–377 (2014).
- ⁴⁷K. Biswas, J. He, I. D. Blum, C.-I. Wu, T. P. Hogan, D. N. Seidman, V. P. Dravid, and M. G. Kanatzidis, "High-performance bulk thermoelectrics with all-scale hierarchical architectures," *Nature* **489**, 414–418 (2012).
- ⁴⁸E. S. Toberer, A. Zevkink, and G. J. Snyder, "Phonon engineering through crystal chemistry," *Journal of Materials Chemistry* **21**, 15843–15852 (2011).
- ⁴⁹J. Ma, V. I. Hegde, K. Munira, Y. Xie, S. Keshavarz, D. T. Mildebrath, C. Wolverton, A. W. Ghosh, and W. Butler, "Computational investigation of half-Heusler compounds for spintronics applications," *Physical Review B* **95**, 024411 (2017).
- ⁵⁰H. C. Kandpal, G. H. Fecher, and C. Felser, "Calculated electronic and magnetic properties of the half-metallic, transition metal based Heusler compounds," *Journal of Physics D: Applied Physics* **40**, 1507 (2007).
- ⁵¹P. Blaha, K. Schwarz, G. K. Madsen, D. Kvasnicka, J. Luitz, *et al.*, "wien2k." An augmented plane wave+ local orbitals program for calculating crystal properties (2001).
- ⁵²P. Giannozzi, S. Baroni, N. Bonini, M. Calandra, R. Car, C. Cavazzoni, D. Ceresoli, G. L. Chiarotti, M. Cococcioni, I. Dabo, *et al.*, "Quantum espresso: a modular and open-source software project for quantum simulations of materials," *Journal of physics: Condensed matter* **21**, 395502 (2009).
- ⁵³J. P. Perdew, K. Burke, and M. Ernzerhof, "Generalized gradient approximation made simple," *Physical review letters* **77**, 3865 (1996).
- ⁵⁴F. Tran and P. Blaha, "Accurate band gaps of semiconductors and insulators with a semilocal exchange-correlation potential," *Phys. Rev. Lett.* **102**, 226401 (2009).
- ⁵⁵G. K. Madsen and D. J. Singh, "Boltztrap: a code for calculating band-structure dependent quantities," *Computer Physics Communications* **175**, 67–71 (2006).
- ⁵⁶A. Togo and I. Tanaka, "First principles phonon calculations in materials science," *Scripta Materialia* **108**, 1–5 (2015).
- ⁵⁷C. Kumarasinghe and N. Neophytou, "Band alignment and scattering considerations for enhancing the thermoelectric power factor of complex materials: The case of Co -based half-Heusler alloys," *Physical Review B* **99**, 195202 (2019).
- ⁵⁸L. Zhang, M.-H. Du, and D. J. Singh, "Zintl-phase compounds with SnSb_4 tetrahedral anions: Electronic structure and thermoelectric properties," *Physical Review B* **81**, 075117 (2010).
- ⁵⁹C. Fu, H. Wu, Y. Liu, J. He, X. Zhao, and T. Zhu, "Enhancing the figure of merit of heavy-band thermoelectric materials through hierarchical phonon scattering," *Advanced Science* **3**, 1600035 (2016).
- ⁶⁰A. Hori, S. Minami, M. Saito, and F. Ishii, "First-principles calculation of lattice thermal conductivity and thermoelectric figure of merit in ferromagnetic half-Heusler alloy CoMnSb ," *Applied Physics Letters* **116**, 242408 (2020).
- ⁶¹S. Mishra, S. Satpathy, and O. Jepsen, "Electronic structure and thermoelectric properties of bismuth telluride and bismuth selenide," *Journal of Physics: Condensed Matter* **9**, 461 (1997).
- ⁶²Y. Min, J. W. Roh, H. Yang, M. Park, S. I. Kim, S. Hwang, S. M. Lee, K. H. Lee, and U. Jeong, "Surfactant-free scalable synthesis of Bi_2Te_3 and Bi_2Se_3 nanoflakes and enhanced thermoelectric properties of their nanocomposites," *Advanced Materials* **25**, 1425–1429 (2013).
- ⁶³B. Lenoir, M. Cassart, J.-P. Michenaud, H. Scherrer, and S. Scherrer, "Transport properties of Bi -rich Bi-Sb alloys," *Journal of Physics and Chemistry of Solids* **57**, 89–99 (1996).
- ⁶⁴T. Fang, F. Li, Y. Wu, Q. Zhang, X. Zhao, and T. Zhu, "Anisotropic thermoelectric properties of n -type Te -free $(\text{Bi}, \text{Sb})_2\text{Se}_3$ with orthorhombic structure," *ACS Applied Energy Materials* **3**, 2070–2077 (2020).